RESEARCH ARTICLE

Vortex-pair states in spin-orbit-coupled Bose–Einstein condensates with coherent coupling

Yong-Kai Liu[1,†], Hong-Xia Yue[1], Liang-Liang Xu[2], Shi-Jie Yang[2,‡]

[1] *College of Physics and Information Engineering, Shanxi Normal University, Linfen 041004, China*
[2] *Department of Physics, Beijing Normal University, Beijing 100875, China*
Corresponding authors. E-mail: †liuyongkai86@163.com, ‡yangshijie@tsinghua.org.cn

Three types of vortex-pair are identified in two-component Bose–Einstein condensates (BEC) of different kinds of spin-orbit coupling. One type holds the two vortices in one component of the two-component condensates. Both the other two types hold a vortex in each component of the two-component condensates, and exhibit meron-pair textures that have either null or unit topological charge, respectively. The cores of the two vortices are connected by a string of the relative phase jump. These vortex pairs can be generated from a vortex-free wave packet by incorporating different non-Abelian gauge field into the BEC. When a Rabi coupling is introduced, the distance between the two cores is effectively controlled by the Rabi coupling strength and a transition of vortex configurations is observed.

1 Introduction

Spin-orbit coupling (SOC) which characterizes the coupling between the spin and the motion degrees of freedom of a particle, plays a key role in many novel quantum phenomena, including quantum anomalous Hall effect, topological insulators, topological superconductors and topological semimetal [1–6]. Unlike electrons in solid state materials, the ultracold atoms do not have intrinsic SO coupling. Synthetic SOC can be generated for ultracold atoms by utilizing atom-light interactions [7]. Multi-component BEC with SOC is highly tunable and provide an ideal platform for quantum simulation and exploring novel quantum phenomena [8, 9]. An important progress was made in the recent experimental realization of two-dimensional (2D) SOC for BEC [10–12].

Many theoretical works on 2D spin-orbit coupled BEC have been extensively studied in cold atom physics [13–17]. The interplay of the SO coupling and the mean-field BEC nonlinearity gives rise to a rich phase diagram in a trapped BEC. The phase diagram is characterized by four different phases [13]. Through increasing interaction, the ground state supports the 1/2-vortex state, the 3/2-vortex state, vortex-lattice state as well as vortex-stripe state. Considering the effect of spin-dependent interactions [14, 15], the ground state falls into two classes of quantum phases, I and II, which respectively preserving the parity (P) and parity-time-reversal (PT) symmetries. Half-quantum vortex state in the phase I is the ground state if the intra-species interaction is weaker than the inter-species interaction and if the interaction strength is below a threshold. Otherwise, it becomes energetically unstable towards a superposition state of two degenerate half-quantum vortex state (the phase IIA), or a state involving higher-order angular momentum (the phase IIB) [15]. With the appropriate SO coupling strength, the half-quantum vortex state forms a skyrmion texture provided appropriate boundary condition is satisfied [15, 17]. However, the study of spin vector and topological property of superposition state of two degenerate half-quantum vortex states is missing.

2D topological structure is a subject of interest in BEC studies for the protection that arises from their topological nontriviality. The topological excitations in spinor condensates are classified by the homotopy class of the order parameter (OP) space [18]. This examination can be carried out with the homotopy group theory [19]. For

example, the 2D skyrmion is classified by the second homotopy group $\pi_2(M)$, where M is the OP manifold [20]. 2D skyrmions have been studied in a wide variety of systems [21–24]. In particular, the spinor condensates have provided an ideal platform to explore the various types of the skyrmions, such as the 2D skyrmion, the half-skyrmion and meron-pair [25–27]. Experimental interests in topological defects and textures are currently accelerating.

In this work, we explore various vortex-pair states in two-component BECs with different kinds of spin-orbit coupling by numerically solving the mean-field Gross-Pitaevskii equation (GPE). There are already various proposals to achieve a nonabelian gauge field. The previous studies are focused on either the Rashba-type or the Dresselhaus-type SOC. Other forms of SOC such as $p_x\hat{\sigma}_y + p_y\hat{\sigma}_z$ are also proposed in Refs. [28–31]. The structures differing in the density distribution and/or phase distribution exhibit different spin texture. We reveal that for the Rashba SOC in weakly interacting spin-1/2 Bose gas, superposition state of two degenerate half-quantum vortex states has a meron-pair spin-texture, i.e., a half-skyrmion and an anti-half-skyrmion, but with null topological charge. It is different from the usual 2D bimeron which was first studied in rotating two-component Bose–Einstein condensates with Rabi coupling [26, 27]. We also study the states in other forms of SO coupling, 2D bimeron with a unit topological charge is created. This supports another way to create 2D bimeron in BEC. We also find a structure that two vortices are created in one component of the BECs. The stability of the three types of vortex-pair is investigated by incorporating a Rabi coupling. It provides a perspective to study the meron-pair and observe the dynamics in BECs.

The paper is organized as follows. In Section 2, the model Hamiltonian is introduced. In Section 3, we study the phase distribution and spin texture in different forms of SO coupled BEC. Three types of vortex-pair with either null or unit topological charge are created. In Section 4, an analysis about the different spin texture is introduced with the concept of the helical modulation. In Section 5, the effect of Rabi coupling is considered and a relation for the structures is revealed. A brief summary is included in Section 6.

2 Model

We consider a 2D pseudo-spin-1/2 boson system confined in a harmonic potential. The condensates are subjected to the different forms of SOC and Rabi coupling. We employ the mean-field approximation and the state of the system is described by the spinor order parameter $\psi(\boldsymbol{r}) = (\psi_1(\boldsymbol{r}), \psi_2(\boldsymbol{r}))^{\mathrm{T}} = (\sqrt{\rho_1(\boldsymbol{r})}\mathrm{e}^{\mathrm{i}\theta_1(\boldsymbol{r})}, \sqrt{\rho_2(\boldsymbol{r})}\mathrm{e}^{\mathrm{i}\theta_2(\boldsymbol{r})})^{\mathrm{T}}$ [32]. The Hamiltonian is written as

$$\mathcal{H} = \int \mathrm{d}^2\boldsymbol{r}\,\psi^\dagger(\boldsymbol{r})\left[\frac{(\boldsymbol{k}^2 + 2\boldsymbol{k}\cdot\boldsymbol{A})}{2m} + \frac{1}{2}m\omega^2 r^2 - \omega_R\sigma_x\right]\psi(\boldsymbol{r})$$
$$+ g_1\hat{n}_1^2(\boldsymbol{r}) + g_2\hat{n}_2^2(\boldsymbol{r}) + 2g_{12}\hat{n}_1(\boldsymbol{r})\hat{n}_2(\boldsymbol{r}), \tag{1}$$

where m is the mass of the atoms and ω is the frequency of the trapping potential. $\hat{n}_1(\boldsymbol{r}) = \psi_1^\dagger(\boldsymbol{r})\psi_1(\boldsymbol{r})$ and $\hat{n}_2(\boldsymbol{r}) = \psi_2^\dagger(\boldsymbol{r})\psi_2(\boldsymbol{r})$ are the density operators for spin-up and spin-down atoms, respectively. $g_j = 4\pi a_j\hbar^2/m$ ($j = 1, 2$) and $g_{12} = 2\pi a_{12}\hbar^2/m$ represent the intra- and inter-component coupling strengths [33]. ω_R is the Rabi frequency and $\boldsymbol{A}$ is a non-Abelian gauge field. The Rashba SOC term is given by $\boldsymbol{A} = \kappa(\sigma_x\hat{x} - \sigma_y\hat{y})$. We intend to systematically explore the phase distribution and spin texture for the non-trivial half-integer angular momentum state for the Rashba type and other forms of SOC as well. We display different kinds of vortex structure related to the forms of SO coupling. An equivalence of these couplings with the usual Rashba and Dresselhaus couplings can be shown by a rotation in the spin space. One may transform both SOCs into each other by a mirror symmetry $y \leftrightarrow -y$ [13]. However, if we consider $\boldsymbol{A} = \kappa(\sigma_z\hat{x} + \sigma_y\hat{y})$, the coupling is completely different. The single particle spectrum of this type of SOC and its properties are introduced in Ref. [30].

We obtain the dimensionless coupled Gross-Pitaevskii (GP) equations for the dynamics of the system in terms of the variational principle. The condensate wave functions are represented by a normalized complex-valued spinor as [32]

$$\begin{pmatrix} \psi_1(\boldsymbol{r}) \\ \psi_2(\boldsymbol{r}) \end{pmatrix} = \sqrt{\rho(\boldsymbol{r})}\mathrm{e}^{\mathrm{i}\Theta(\boldsymbol{r})}\begin{pmatrix} \chi_1(\boldsymbol{r}) \\ \chi_2(\boldsymbol{r}) \end{pmatrix}, \tag{2}$$

with $|\chi_1(\boldsymbol{r})|^2 + |\chi_2(\boldsymbol{r})|^2 = 1$. The total density is $\rho(\boldsymbol{r}) = \rho_1(\boldsymbol{r}) + \rho_2(\boldsymbol{r})$ and the overall and relative phase are $\Theta(\boldsymbol{r}) = (\theta_1(\boldsymbol{r}) + \theta_2(\boldsymbol{r}))/2$, $\phi(\boldsymbol{r}) = \theta_2(\boldsymbol{r}) - \theta_1(\boldsymbol{r})$.

The pseudospin density is defined by $\boldsymbol{S}(\boldsymbol{r}) = \chi^\dagger(\boldsymbol{r})\hat{\sigma}\chi(\boldsymbol{r})$. The explicit expressions of $\boldsymbol{S} = (S_x, S_y, S_z)$ are given by $S_x = \chi_1^*\chi_2 + \chi_2^*\chi_1 = \sin\theta\cos\phi$, $S_y = -\mathrm{i}(\chi_1^*\chi_2 - \chi_2^*\chi_1) = \sin\theta\sin\phi$, and $S_z = |\chi_1|^2 - |\chi_2|^2 = \cos\theta$, where $\sigma = (\sigma_x, \sigma_y, \sigma_z)$ are the Pauli matrices and $\cos\theta = (\rho_2 - \rho_1)/\rho$. The superfluid velocity is $v_{\mathrm{mass}} = \frac{\hbar}{m}\nabla\frac{\theta_1 + \theta_2}{2}$, and the flux flow of the spinor is $v_{\mathrm{spin}} = \frac{\hbar}{m}\cos\theta\nabla\frac{\theta_1 - \theta_2}{2}$ [32]. The vortex winding number is defined by the superfluid velocity integrating along a closed path enclosing all the vortices. If the vortex has a fountain texture in $\boldsymbol{S}(\boldsymbol{r})$, it corresponds to 2D topological structure, e.g, 2D skyrmion. In order to describe the distribution of the 2D topological structure, a topological charge defined in a 2D system as $Q = \frac{1}{4\pi}\int q(\boldsymbol{r})\mathrm{d}x\mathrm{d}y$, with charge density $q(\boldsymbol{r}) = \boldsymbol{S}(\boldsymbol{r})\cdot(\partial_x\boldsymbol{S}(\boldsymbol{r})\times\partial_y\boldsymbol{S}(\boldsymbol{r}))$. We numerically solve the dimensionless coupled GP equations by using the imaginary-time propagation method based on the pseudo-spectral method [34, 35].

3 Vortex-pairs in different forms of SOC

Different kinds of couplings between the spin and linear momentum may have different consequence on the distribution of the condensate wave functions both in density and phase, which result in different spin textures. The situations are more complex when the interactions are taken into account. We consider $p_x\hat{\sigma}_z + p_y\hat{\sigma}_y$ as the form of spin-orbit coupling in the two-component BECs. The numerical simulations confirm that two types of vortex-pair are indeed created(Type II and Type III), which is different from the vortex-pair in the Rashba SOC(Type I).

3.1 Type I

First we review the condensate with the 2D Rashba SOC. The phase diagram of a Rashba spin-orbit coupled spinor BEC have been investigated by using mean-field theory for $(g_{12} = g)$ [13] and $(g_{12} \neq g)$ [14]. For a weakly interacting, the half-vortex solution corresponds to two states, namely, IA and IIA, which differ in the density distribution. The critical interaction strength g_c increases rapidly with decrease of the SO coupling strength. With the appropriate SO coupling strengths, the half-quantum vortex state IA forms a skyrmion-type texture so far as the boundary condition is satisfied [15]. The increase of the SO coupling leads to more oscillations in the radial direction [17].

In the present work, we first investigate the half-vortex solution IIA which is a superposition state of two degenerate half-quantum vortex states in the Rashba SOC [15]. However, in Ref. [15], the discussion about the phase and the topological property is missing. Figure 1 shows the density distributions [(a)–(c)] and the phase distributions [(d)–(f)]. We observe that the density distribution of the IIA state is the same as the 2D bimeron in rotating two-component Bose–Einstein condensates with Rabi coupling. Each component has one off-axis vortex and the density peak of one component is locked at the vortex core of the other component. The profile of the relative phase plays an important role in optimizing the vortex structure, as shown in Fig. 1(f). The pair of vortices has circulation of opposite sign in each individual phase space [Figs. 1(d), (e)] and the total relative phase accumulated along a loop encircling the two vortices is 4π [Fig. 1(f)], which is different from the 2D bimeron situation (Type III).

In the absence of SOC. the 2D bimeron is usually stabilized by the coherent Rabi coupling [26, 27]. The cores of the two vortices are connected by a domain wall of the relative phase to form a vortex-molecule. Essentially, the coherent Rabi coupling plays the role of a transverse magnetic field that aligns the spin along the x-axis, leading to $\chi^{\dagger} \to (1, 1)$ at distances far from the core region. To gain more insights of the superposition state, it is useful to study the spin texture and the topological charge density, which is shown in Figs. 4(a) and (b). It is readily seen that the spin vector twists in space and forms a half-skyrmion and anti-half-skyrmion texture. The distribution is odd with respect to the x-axis [Fig. 4(b)], which emphasizes the creation of a meron-antimeron pair with a vanishing total topological charge. In our calculations, $Q = \int q(\boldsymbol{r})\mathrm{d}x\mathrm{d}y = \frac{1}{2} + (-\frac{1}{2}) = 0$.

3.2 Type II

Next, we study $p_x\hat{\sigma}_z + p_y\hat{\sigma}_y$ as the form of SOC in two-component BECs with spinor $(1,0)^{\mathrm{T}}$ as the initial state. We denote the positions of the vortices in spin-up component as $(-x_m, x_m)$. In Fig. 2, it is shown that $|\psi_1(\boldsymbol{r})|^2$ vanishes at two off-centered location, at which the $|\psi_2(\boldsymbol{r})|^2$ reaches its maximum. The two points of vanishing density are located at symmetric positions $x = \pm x_m$. The central and the outermost region is filled by the ψ_1. In addition, the phase of $\psi_1(\boldsymbol{r})$ exhibits two
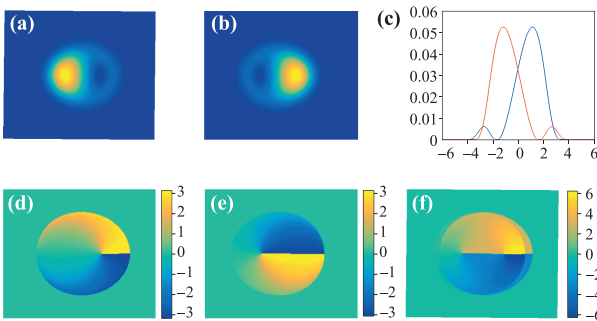

Fig. 1 The density profiles for **(a)** ψ_1 and **(b)** ψ_2. **(c)** The cross sections of $|\psi_1|^2$ and $|\psi_2|^2$ along the x axis at $y = 0$. The phase distribution for **(d)** ψ_1 and for **(e)** ψ_2. **(f)** The plot of the relative phase. $g_1 = g_2 = 79$, $g_{12} = 70$ and $\kappa = 0.9$.
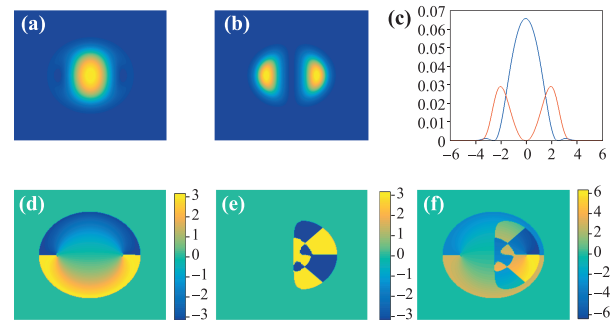

Fig. 2 The same as in Fig. 1 for 2D configuration of Type II. $g_1 = g_2 = g_{12} = 79$ and $\kappa = 1.05$. A vortex-free Gaussian wave packet with uniform spinor $(1, 0)^{\mathrm{T}}$ as the initial state.

clear 2π phase winding around the core. They form a vortex-antivortex pair. The total phase winding along a loop encircling the two vortices (the total vortex winding number) is zero. It is notable that the density and phase profile are the same as the conventional 2D skyrmion for each half plane, where one component is located at the vortex core of the other component. It is just like two conventional 2D skyrmion put together. As the phase of ψ_{-1} jumps from 0 to π, the ψ_{-1} shows a dark soliton state. The spin texture is shown in Fig. 4(c).

The topological charge density is odd with respect to the x-coordinate like type I which reveals the creation of a meron-antimeron pair with vanishing total topological charge $Q = \int q(\boldsymbol{r})\mathrm{d}x\mathrm{d}y = \frac{1}{2} + (-\frac{1}{2}) = 0$.

3.3 Type III

After sufficiently long imaginary-time propagation with spinor $(1/\sqrt{2}, -1/\sqrt{2})^{\mathrm{T}}$ as the initial state, we obtain the stable bimeron state, as shown in Fig. 3. In contrast to Type I and Type II, this pair of vortices has circulation of the same sign in each individual phase space, but has the opposite sign in the relative phase space. The profile of the relative phase plays an important role in optimizing the structure, which is shown in Fig. 3(f). The pseudospin S orientations depend on the relative phase, which can be represented by an azimuthal angle $\arctan(S_y/S_x) = \theta_2(\boldsymbol{r}) - \theta_1(\boldsymbol{r})$ [26, 27]. The two vortices are connected by a topological sine-Gordon soliton which is also called as a magnetic domain wall. The domain wall has the relative phase with the 2π difference. Then the vortex in one component and that in the other component can be bound by the domain wall, forming a vortex molecule. The total 2D topological charge is $Q = \int q(\boldsymbol{r})\mathrm{d}x\mathrm{d}y = \frac{1}{2} + \frac{1}{2} = 1$ and the spin texture is shown in Fig. 4(d).

We have verified that the obtained solution is the true ground state from a variety of initial conditions. We compare the energy of Type II and Type III and we find the
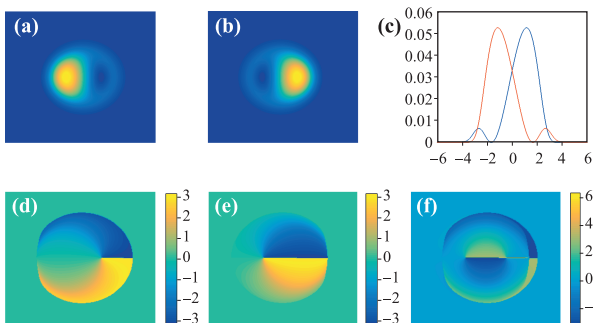

Fig. 3 The same as in Fig. 1 for 2D configuration of Type III. $g_1 = g_2 = g_{12} = 79$ and $\kappa = 0.9$. A vortex-free Gaussian wave packet with uniform spinor $(1/\sqrt{2}, -1/\sqrt{2})^{\mathrm{T}}$ as the initial state.
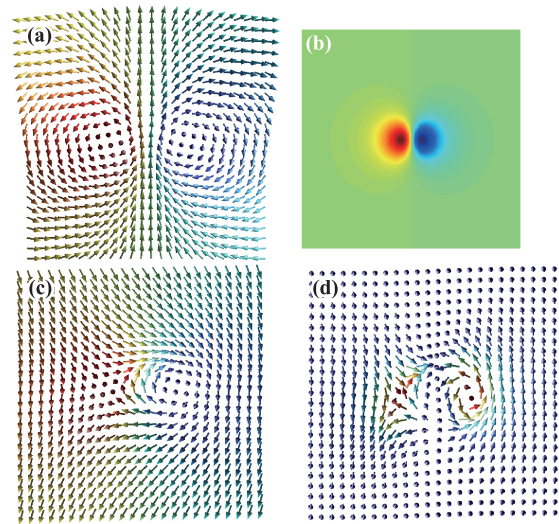

Fig. 4 The spin-textures for **(a)** Type I **(c)** Type II and **(d)** Type III. The corresponding topological charge density for **(b)** Type I.

two solutions are degenerated for $g_1 = g_2 = g_{12}$. Type II structure is the ground state if the intra-species interaction is smaller than the inter-species interaction and if the interaction strength is below a threshold. Type III structure is the ground state if the intra-species interaction is larger than the inter-species interaction and if the interaction strength is below a threshold.

4 Theoretical analysis

The emerged vortex-pair are physically understandable with the concept of the helical OP modulation. For the SO-coupled BEC, the Hamiltonian $\mathcal{H}$ is invariant under the simultaneous $SO(2)$ global spin-space rotations. The concept of the helical modulation of the OP [36, 37] provides a good method to understand the structure under the non-Abelian gauge field. Based on the theory, the OP under a non-Abelian gauge field can be written with the rotation matrix $V = \exp(-\mathrm{i}\varphi\boldsymbol{n}\cdot\boldsymbol{\sigma})$ acts on an arbitrary $\psi(\boldsymbol{r}_0)$ around the unit vector $\boldsymbol{n}$ by the angle φ. The non-Abelian gauge field favors the situation where the rotation axis $\boldsymbol{n}$ corresponds to the modulation vector $\boldsymbol{h}$ [37].

For the non-Abelian gauge field, the rotation matrix $V_1 = \exp(-\mathrm{i}\varphi[\sigma_x n_x + \sigma_y n_y])$ for the Rashba-Dresselhaus type SOC and the rotation matrix $V_2 = \exp(-\mathrm{i}\varphi[\sigma_z n_x + \sigma_y n_y])$ for the other form of SOC. From the analysis of single particle spectrum E_0 of an ideal Bose gas, E_0 has a minimum line along $\sqrt{k_x^2 + k_y^2}$ as presented in Ref. [36]. Therefore, it turns out that the possible stable texture is the helical spin modulation with

the vector $\boldsymbol{h}//(k_x, k_y, 0)$ in the x–y plane. This results in the different texture with the appropriate $\varphi \sim \boldsymbol{k} \cdot \boldsymbol{r}$ to fulfill the OP manifold according to the different wave functions [36–38]. For the Rashba type of SO coupling, the appropriate $\varphi \sim \boldsymbol{k} \cdot \boldsymbol{r}$ can result in the rotation matrix V_1 becoming U_1. The corresponding 2D skyrmion and meron-pair (Type I) are created, when U_1 acts on the representative spinor $(1, 0)^{\mathrm{T}}$ and $(1/\sqrt{2}, -1/\sqrt{2})^{\mathrm{T}}$.

In order to better understand this theory, we can approximately consider the OP of a two-component BEC for a rotationally symmetric configuration of a 2D skyrmion (representative spinor $(1, 0)^{\mathrm{T}}$) and Type I meron-pair with representative spinor $(1/\sqrt{2}, -1/\sqrt{2})^{\mathrm{T}}$,

$$\begin{pmatrix} \psi_1(\boldsymbol{r}) \\ \psi_2(\boldsymbol{r}) \end{pmatrix} = \sqrt{n(\boldsymbol{r})} U_1(\boldsymbol{r}) \begin{pmatrix} 1 \\ 0 \end{pmatrix} \quad \text{or} \quad \begin{pmatrix} 1/\sqrt{2} \\ -1/\sqrt{2} \end{pmatrix}, \quad (3)$$

where $U_1(\boldsymbol{r}) = \exp\left[-i\lambda(\boldsymbol{r})(\sigma_x n_x + \sigma_y n_y)\right]$. $U(\boldsymbol{r})$ defines a mapping from the compactified 2D physical region to the order parameter space. The map falls into the homotopy class which is characterized by the homotopy group $\pi_2(S^2) = Z$. It is illustrative to study the topological structure with the radial symmetric ansatz by assuming $\lambda(0) = \pi$ and $\lambda(\infty) = 0$ with $\boldsymbol{n} = (n_x, n_y, 0) = (\cos\theta, \sin\theta, 0)$. And we can get the 2D winding number $Q_{2D} = 1$ for 2D skyrmion and $Q = \frac{1}{2} + (-\frac{1}{2}) = 0$ for Type I meron-pair.

For the type of SO coupling $(p_x \hat{\sigma}_z + p_y \hat{\sigma}_y)$, the appropriate $\varphi \sim \boldsymbol{k} \cdot \boldsymbol{r}$ can result in the rotation matrix V_2 becoming U_2. The corresponding vortex-pair in one component (Type II) and in two component (the 2D bimeron Type III) are created, when U_2 acts on the representative spinor $(1, 0)^{\mathrm{T}}$ and $(1/\sqrt{2}, -1/\sqrt{2})^{\mathrm{T}}$. For this case, we can approximately consider the OP of a two-component BEC as

$$\begin{pmatrix} \psi_1(\boldsymbol{r}) \\ \psi_2(\boldsymbol{r}) \end{pmatrix} = \sqrt{n(\boldsymbol{r})} U_2(\boldsymbol{r}) \begin{pmatrix} 1 \\ 0 \end{pmatrix} \quad \text{or} \quad \begin{pmatrix} 1/\sqrt{2} \\ -1/\sqrt{2} \end{pmatrix}, \quad (4)$$

where $U_2(\boldsymbol{r}) = \exp\left[-i\lambda(\boldsymbol{r})(\sigma_z n_x + \sigma_y n_y)\right]$. A rotationally symmetric configuration can also be given as before.

We find that all the ansatz wave functions indeed give the same distribution of the density, phase and spin texture as our work in SOC. It verifies the correctness of our previous results for the structural analysis.

5   Effects of Rabi coupling

Coherent Rabi coupling between the two component BECs is experimentally achieved by the JILA group [39]. The coherent coupling term with the Rabi frequency acts as a transverse magnetic field that aligns the spin along the x-axis. This interaction couples the atoms of the two components via the relative phase of the order parameters. Since the two-component BECs are coupled by the

uniform coherent Rabi coupling, one cannot make a vortex in one of the components without affecting the phase in the other component. The relative phase between the two components prefers to be uniform to reduce the coupling energy.

We study the interplay between the Rabi interaction and SOC interaction on the vortex-pair structure. For meron-pair (Type I and Type III), the increase of the Rabi frequency ω_R induces the decrease of the size of the meron pair (the separation distance of the vortex core). This indicates that the binding of the meron-pair becomes stronger. We also note that the magnitude of decreasing in the size of the meron pair with increase of the SOC is small and may bring in new vortices. Consequently, the size of the meron pair are effectively controlled by the strength of the Rabi coupling.

While 2D skyrmion can be created in rotating two-component Bose–Einstein condensates, 2D bimeron is created by switching on the Rabi term. It is equivalent to the effect that rotates the spinor as $\psi_\pm^{bimeron} = \frac{\sqrt{2}}{2}(\psi_1^{skyrmion} \pm \psi_2^{skyrmion})$.

In our model, 2D skyrmion ($Q = 1$) is created in the Rashba SOC. As the Rabi coupling is implemented, the meron-pair (Type I, $Q = 0$) instead of 2D bimeron (Type III, $Q = 1$) is created. The vortex-pair (Type II, $Q = 0$) can be created in other form of SOC and 2D bimeron (Type III, $Q = 1$) is created when the Rabi coupling is considered. We can see that the Rabi interaction indeed couple the two component. However, the form of combination is also effected by the forms of the SOC, differing to the case in rotating two-component Bose–Einstein condensates. Notably, if we choose the skyrmion ($Q = 1$) as the initial state in forms of SOC $(p_x \hat{\sigma}_z + p_y \hat{\sigma}_y)$ with Rabi coupling, 2D bimeron (Type III, $Q = 1$) is created. If we choose the vortex-pair (Type II, $Q = 0$) as the initial state in Rashba SOC with Rabi coupling, meron-pair (Type I, $Q = 0$) is created. It provides us an ideal model to study the dynamics of the transition of the different structure with the same topological charge.

6   Summary

We have studied and proposed methods for creating three types of vortex-pair in two-component BEC. The first one (Type I) with total topological charge 0, has circulation of the opposite sign in each individual phase space, which can be created by incorporating a Rashba type spin-orbit coupling into BEC. The second one (Type II) has total topological charge 0 and holds a pair of a vortex and an antivortex in the same component, which can be created by incorporating a non-Abelian gauge potential $(p_x \hat{\sigma}_z + p_y \hat{\sigma}_y)$ into BEC. The third one (Type III) is a 2D bimeron with the one topological charge, which

can be created by incorporating a non-Abelian gauge potential $(p_x \hat{\sigma}_z + p_y \hat{\sigma}_y)$ into BEC. We also examine the effect of the Rabi coupling on the vortex-pair, and a relation between them is revealed.

References

1. D. C. Tsui, H. L. Stormer, and A. C. Gossard, Two-dimensional magnetotransport in the extreme quantum limit, *Phys. Rev. Lett.* 48(22), 1559 (1982)

2. I. Zutic, J. Fabian, and S. Das Sarma, Spintronics: Fundamentals and applications, *Rev. Mod. Phys.* 76(2), 323 (2004)

3. M. Z. Hasan and C. L. Kane, Topological insulators, *Rev. Mod. Phys.* 82(4), 3045 (2010)

4. X. L. Qi and S. C. Zhang, Topological insulators and superconductors, *Rev. Mod. Phys.* 83(4), 1057 (2011)

5. F. Wilczek, Majorana returns, *Nat. Phys.* 5(9), 614 (2009)

6. X. Wan, A. M. Turner, A. Vishwanath, and S. Y. Savrasov, Topological semimetal and Fermi-arc surface states in the electronic structure of pyrochlore iridates, *Phys. Rev. B* 83(20), 205101 (2011)

7. Y. J. Lin, K. Jiménez-García, and I. B. Spielman, Spin-orbit-coupled Bose–Einstein condensates, *Nature* 471(7336), 83 (2011)

8. S. W. Song, L. Wen, C. F. Liu, S. C. Gou, and W. M. Liu, Ground states, solitons and spin textures in spin-1 Bose–Einstein condensates, *Front. Phys.* 8(3), 302 (2013)

9. Y. Li and J. K. Xue, Stationary and moving solitons in spin-orbit-coupled spin-1 Bose–Einstein condensates, *Front. Phys.* 13(2), 130307 (2018)

10. L. Huang, Z. Meng, P. Wang, P. Peng, S. Zhang, L. Chen, D. Li, Q. Zhou, and J. Zhang, Experimental realization of two-dimensional synthetic spin-orbit coupling in ultracold Fermi gases, *Nat. Phys.* 12(6), 540 (2016)

11. Z. Wu, L. Zhang, W. Sun, X. Xu, B. Wang, S. Ji, Y. Deng, S. Chen, X. Liu, and J. Pan, Realization of two-dimensional spin-orbit coupling for Bose–Einstein condensates, *Science* 354(6308), 83 (2016)

12. W. Sun, B. Wang, X. Xu, C. Yi, L. Zhang, Z. Wu, Y. Deng, X. Liu, S. Chen, and J. Pan, Long-lived 2D Spin-Orbit coupled Topological Bose Gas, arXiv: 1710.00717 (2017)

13. S. Sinha, R. Nath, and L. Santos, Trapped two-dimensional condensates with synthetic spin-orbit coupling, *Phys. Rev. Lett.* 107(27), 270401 (2011)

14. H. Hu, B. Ramachandhran, H. Pu, and X. J. Liu, Spin-orbit coupled weakly interacting Bose–Einstein condensates in harmonic traps, *Phys. Rev. Lett.* 108(1), 010402 (2012)

15. B. Ramachandhran, B. Opanchuk, X. J. Liu, H. Pu, P. D. Drummond, and H. Hu, Half-quantum vortex state in a spin-orbit-coupled Bose–Einstein condensate, *Phys. Rev. A* 85(2), 023606 (2012)

16. C. Wang, C. Gao, C. M. Jian, and H. Zhai, Spin-orbit coupled spinor Bose–Einstein condensates, *Phys. Rev. Lett.* 105(16), 160403 (2010)

17. X. Zhou, Y. Li, Z. Cai, and C. Wu, Unconventional states of bosons with the synthetic spin-orbit coupling, *J. Phys. At. Mol. Opt. Phys.* 46(13), 134001 (2013)

18. Y. Kawaguchi and M. Ueda, Spinor Bose–Einstein condensates, *Phys. Rep.* 520(5), 253 (2012)

19. H. Mäkelä, Explicit expressions for the topological defects of spinor Bose–Einstein condensates, *J. Phys. Math. Gen.* 39(23), 7423 (2006)

20. K. Kasamatsu, H. Takeuchi, M. Tsubota, and M. Nitta, Wall-vortex composite solitons in two-component Bose–Einstein condensates, *Phys. Rev. A* 88(1), 013620 (2013)

21. T. A. Skyrme, A unified field theory of mesons and baryons, *Nucl. Phys.* 31, 556 (1962)

22. Y. M. Cho, Monopoles and knots in Skyrme theory, *Phys. Rev. Lett.* 87(25), 252001 (2001)

23. S. L. Sondhi, A. Karlhede, S. A. Kivelson, and E. H. Rezayi, Skyrmions and the crossover from the integer to fractional quantum Hall effect at small Zeeman energies, *Phys. Rev. B* 47(24), 16419 (1993)

24. N. Romming, C. Hanneken, M. Menzel, J. E. Bickel, B. Wolter, K. von Bergmann, A. Kubetzka, and R. Wiesendanger, Writing and deleting single magnetic skyrmions, *Science* 341(6146), 636 (2013)

25. Y. Kawaguchi, M. Kobayashi, M. Nitta, and M. Ueda, Topological excitations in spinor Bose–Einstein condensates, *Prog. Theor. Phys. Suppl.* 186, 455 (2010)

26. K. Kasamatsu, M. Tsubota, and M. Ueda, Spin textures in rotating two-component Bose–Einstein condensates, *Phys. Rev. A* 71(4), 043611 (2005)

27. K. Kasamatsu, M. Tsubota, and M. Ueda, Vortex molecules in coherently coupled two-component Bose–Einstein condensates, *Phys. Rev. Lett.* 93(25), 250406 (2004)

28. T. D. Stanescu, C. Zhang, and V. Galitski, Nonequilibrium spin dynamics in a trapped fermi gas with effective spin-orbit interactions, *Phys. Rev. Lett.* 99(11), 110403 (2007)

29. J. Ruseckas, G. Juzeliunas, P. Ohberg, and M. Fleischhauer, Non-Abelian gauge potentials for ultracold atoms with degenerate dark states, *Phys. Rev. Lett.* 95(1), 010404 (2005)

30. T. Stanescu, B. Anderson, and V. Galitski, Spin-orbit coupled Bose–Einstein condensates, *Phys. Rev. A* 78(2), 023616 (2008)

130316-6

Yong-Kai Liu, et al., Front. Phys. 13(5), 130316 (2018)

31. J. Radić, T. A. Sedrakyan, I. B. Spielman, and V. Galitski, Vortices in spin-orbit-coupled Bose–Einstein condensates, *Phys. Rev. A* 84(6), 063604 (2011)

32. K. Kasamatsu, H. Takeuchi, M. Tsubota, and M. Nitta, Wall-vortex composite solitons in two-component Bose–Einstein condensates, *Phys. Rev. A* 88(1), 013620 (2013)

33. H. Wang, L. Wen, H. Yang, C. Shi, and J. Li, Vortex states and spin textures of rotating spin-orbit-coupled Bose–Einstein condensates in a toroidal trap, *J. Phys. At. Mol. Opt. Phys.* 50(15), 155301 (2017)

34. W. Bao, D. Jaksch, and P. A. Markowich, Numerical solution of the Gross–Pitaevskii equation for Bose–Einstein condensation, *J. Comput. Phys.* 187(1), 318 (2003)

35. W. Bao and H. Wang, An efficient and spectrally accurate numerical method for computing dynamics of rotating Bose–Einstein condensates, *J. Comput. Phys.* 217(2), 612 (2006)

36. T. Kawakami, T. Mizushima, M. Nitta, and K. Machida, Stable skyrmions in $SU(2)$ gauged Bose–Einstein condensates, *Phys. Rev. Lett.* 109(1), 015301 (2012)

37. T. Kawakami, T. Mizushima, and K. Machida, Textures of $F = 2$ spinor Bose–Einstein condensates with spin-orbit coupling, *Phys. Rev. A* 84, 011607(R) (2011)

38. Y. K. Liu and S. J. Yang, Three-dimensional dimeron as a stable topological object, *Phys. Rev. A* 91(4), 043616 (2015)

39. M. R. Matthews, B. P. Anderson, P. C. Haljan, D. S. Hall, M. J. Holland, J. E. Williams, C. E. Wieman, and E. A. Cornell, Watching a superfluid untwist itself: Recurrence of Rabi oscillations in a Bose–Einstein condensate, *Phys. Rev. Lett.* 83(17), 3358 (1999)

Frontiers of Physics

Yong-Kai Liu, et al., Front. Phys. 13(5), 130316 (2018)

130316-7